

# Josephson $\varphi_0$ -junction in nanowire quantum dots

D. B. Szombati<sup>1</sup>, S. Nadj-Perge<sup>1</sup>, D. Car<sup>2</sup>, S. R. Plissard<sup>3</sup>, E. P. A. M. Bakkers<sup>1,2</sup> and L. P. Kouwenhoven<sup>1\*</sup>

**The Josephson effect describes supercurrent flowing through a junction connecting two superconducting leads by a thin barrier<sup>1</sup>. This current is driven by a superconducting phase difference  $\varphi$  between the leads. In the presence of chiral and time-reversal symmetry of the Cooper pair tunnelling process<sup>2</sup>, the current is strictly zero when  $\varphi$  vanishes. Only if these underlying symmetries are broken can the supercurrent for  $\varphi = 0$  be finite<sup>3–5</sup>. This corresponds to a ground state of the junction being offset by a phase  $\varphi_0$ , different from 0 or  $\pi$ . Here, we report such a Josephson  $\varphi_0$ -junction based on a nanowire quantum dot. We use a quantum interferometer device to investigate phase offsets and demonstrate that  $\varphi_0$  can be controlled by electrostatic gating. Our results may have far-reaching implications for superconducting flux- and phase-defined quantum bits as well as for exploring topological superconductivity in quantum dot systems.**

The process of Cooper pair tunnelling through a Josephson junction (JJ) is, in general, symmetric with respect to time inversion. This has a profound consequence for the JJ current–phase relation,  $I(\varphi)$ . In particular it imposes the condition  $I(-\varphi) = -I(\varphi)$ , which in turn results in  $I(\varphi = 0)$  being strictly zero. The  $I(\varphi = 0) = 0$  condition is a consequence of the fact that for each process contributing to current flowing in one direction there is an opposite time-reversed process, in which spin-up and spin-down electrons are reversed, that exactly cancels this current. However, time inversion is not the only symmetry which can protect the  $I(\varphi = 0) = 0$  condition. For example, in JJs based on single-domain ferromagnets, time inversion is broken, but the supercurrent is still zero for  $\varphi = 0$  owing to chiral symmetry—that is, the symmetry between leftward and rightward tunnelling. This symmetry ensures that the tunnelling coefficient describing the electron tunnelling from the left lead to the right lead is exactly the same as the one describing the tunnelling in reverse, from the right lead to the left lead. The two tunnelling processes (leftward and rightward) cancel each other, which again results in  $I(\varphi = 0)$  being strictly zero. This is even the case for so-called  $\pi$ -junctions<sup>6</sup>, in which the current flow is reversed compared to usual JJs, but still the underlying symmetries guarantee zero current for  $\varphi = 0$ . To create conditions for a non-zero supercurrent to flow at  $\varphi = 0$ , both symmetries need to be broken<sup>7</sup>. Various ways have been proposed theoretically to break the underlying symmetries and create  $\varphi_0$ -junctions, including ones based on non-centrosymmetric or multilayer ferromagnets<sup>3,8</sup>, quantum point contacts<sup>4</sup>, topological insulators<sup>9,10</sup>, diffusive systems<sup>11,12</sup>, nanowires<sup>13,14</sup> and quantum dots<sup>5,15,16</sup>. Alternatively, an effective built-in phase offset can be obtained by combining 0- and  $\pi$ -junctions in parallel<sup>17,18</sup>. However, no experimental demonstration of a  $\varphi_0$ -junction has been reported until now.

In quantum dots (QDs), breaking of both symmetries can be achieved by the combination of an external magnetic field and

the spin–orbit interaction (SOI)<sup>5,15,16</sup>. A finite Zeeman splitting between spin-up and spin-down electrons breaks the time-reversal symmetry. On the other hand, breaking of the chiral symmetry is more subtle. It requires an interplay between the SOI and the magnetic field, and can occur only when multiple orbitals are accessible for electron transport (see Fig. 1a). When an electron goes in and out from the QD via only one orbital (Fig. 1a, upper panel) the tunnelling coefficient is exactly the same for the leftward and the rightward tunnelling direction. In this case the chiral symmetry is preserved. If, however, the electron changes orbital within the quantum dot during the course of tunnelling (Fig. 1a, lower panel), an extra phase factor is acquired in the process of orbital mixing. This phase factor, arising from the SOI-enabled orbital mixing, now depends on the tunnelling direction and is different for the leftward and rightward tunnelling process. As a consequence, the two processes cannot cancel each other, and the chiral symmetry is broken. Although here we discuss the case of a single electron tunnelling through the QD, the same argument holds for the breaking of the chiral symmetry in the tunnelling of Cooper pairs (see Supplementary Section 1 and ref. 5). Note that in this scenario both symmetries are explicitly broken by the combination of the magnetic field and the SOI<sup>5</sup>.

The device geometry is shown in Fig. 1b,c. A single nanowire, made of indium antimonide (InSb), is contacted using niobium titanium nitride (NbTiN) as a superconductor to make two JJs forming a quantum interference device (SQUID). We choose InSb nanowires owing to their large spin–orbit coupling and  $g$ -factors, both of which are important for breaking time inversion and chiral symmetry at relatively low magnetic fields<sup>19,20</sup>. Electrostatic gates below the wire are used to create a tunable quantum dot in the longer JJ and control the switching current of the shorter reference JJ (ref. 19; Fig. 1b). Our coordinate system is defined such that the in-plane magnetic field coincides with the  $x$ - and  $z$ -axis, whereas the flux through the SQUID is applied along the  $y$ -direction (Fig. 1c). Standard quantum dot characterization, while the reference junction is pinched off, is used to determine the values of the charging ( $E_C$ ) and orbital ( $E_{\text{orb}}$ ) energies as well as  $g$ -factors. Depending on the confinement details and QD occupation number we find  $E_C = 2\text{--}3$  meV,  $E_{\text{orb}} = 0.3\text{--}1.5$  meV and  $g = 40\text{--}50$  (Fig. 1d). We identify small peaks around zero bias as an onset of superconductivity, and estimate the induced superconducting gap in the QD to be  $\Delta^* = 20\text{--}50$   $\mu\text{eV}$  (see Supplementary Section 2).

First we measure the SQUID response in current bias for zero in-plane magnetic field (Fig. 2). Switching currents for the reference and quantum dot JJ,  $I_{\text{ref}}$  and  $I_{\text{cQD}}$ , satisfy  $I_{\text{ref}} \gg I_{\text{cQD}}$ , ensuring that the phase drop is mainly across the QD. The measured voltage as a function of flux and bias current  $I_{\text{bias}}$  shows oscillations with a period of  $B_y = 1.2$  mT (Fig. 2a), corresponding to an effective area of  $1.8$   $\mu\text{m}^2$ , which is consistent with the SQUID geometry and the penetration depth of NbTiN ( $\lambda \approx 170$  nm). Both junctions are in the

<sup>1</sup>QuTech and Kavli Institute of Nanoscience, Delft University of Technology, 2600 GA Delft, The Netherlands. <sup>2</sup>Department of Applied Physics, Eindhoven University of Technology, 5600 MB Eindhoven, The Netherlands. <sup>3</sup>CNRS-Laboratoire d'Analyse et d'Architecture des Systèmes (LAAS), Université de Toulouse, 7 avenue du colonel Roche, F-31400 Toulouse, France. \*e-mail: l.p.kouwenhoven@tudelft.nl

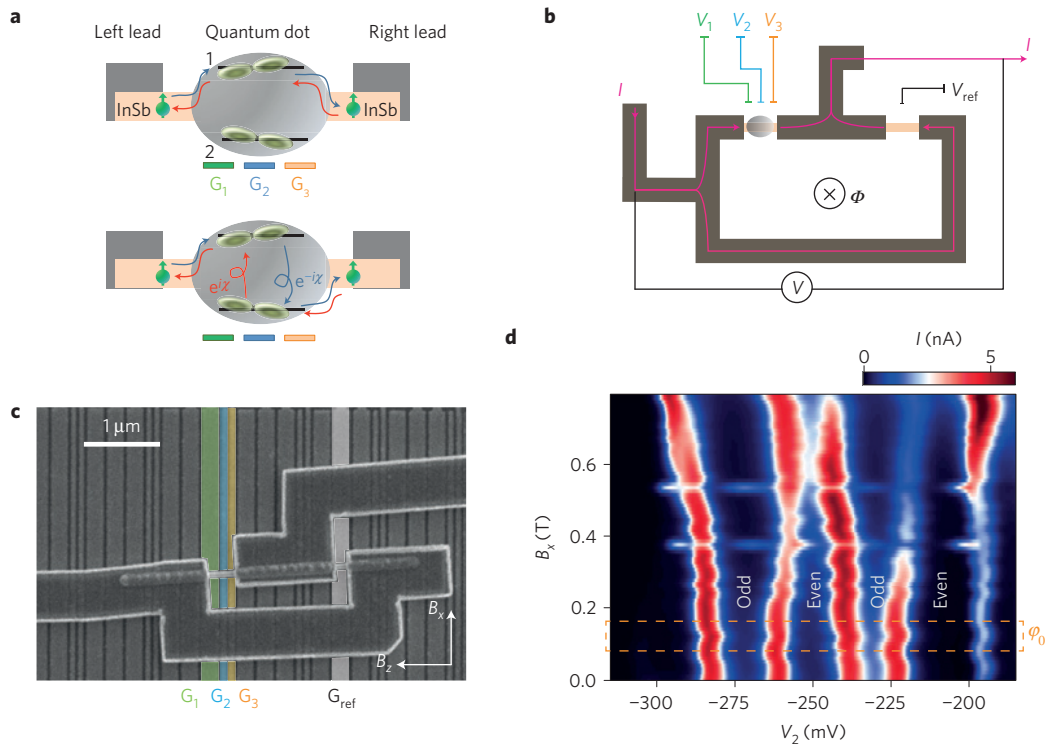


**Figure 1 | Schematics of the experiment.** **a**, Schematics showing tunnelling of an electron through the QD with two orbitals labelled 1 and 2 which are mixed by the SOI. The blue (red) line describes tunnelling of an electron from the left (right) to the right (left) lead. When there is no change in orbital, the two processes cancel each other (upper panel). In contrast, when the orbital is changed during the tunnelling (lower panel), owing to interplay between the SOI and a magnetic field  $B$ , leftward and rightward tunnelling processes do not cancel. In this case an extra phase  $\chi$  is obtained in the process, which depends on both the strength of the SOI and  $B_{\text{in-plane}}$ . Note that the phases for forward and backward tunnelling are opposite. **b**, Device schematic showing a dc-SQUID measured in a four-terminal geometry. Voltages  $V_1, V_2, V_3$  and  $V_{\text{ref}}$  are applied on underlying gates to control the conductance of the JJs. **c**, Scanning electron microscopy (SEM) image of the actual device. Gates  $G_1, G_2$  and  $G_3$  are used to define a quantum dot in the long JJ, while  $G_{\text{ref}}$  tunes the current through the reference JJ. The orientations of the in-plane magnetic fields  $B_x$  and  $B_z$  are marked.  $B_y$  is used for tuning the flux  $\Phi$  through the SQUID. **d**, Current as a function of  $V_2$  and  $B_x$  showing QD evolution of the Coulomb peak spacing in the field which gives  $g_x \approx 51$ . From similar data, taken for  $B_z$ , we obtain  $g_z \approx 44$ , and estimate the level repulsion between different spin configurations due to the SOI of  $\Delta_{\text{SO}} \approx 170 \mu\text{eV}$ . The extracted  $\Delta_{\text{SO}}$  corresponds to a spin-orbit length  $l_{\text{so}} \approx 350 \text{ nm}$  and a spin-orbit energy  $E_{\text{SO}} \approx 20 \mu\text{eV}$ , comparable to previous QD experiments<sup>19</sup>. Measurements are performed in the voltage bias regime,  $V_{\text{bias}} = 500 \mu\text{V}$ . The dashed rectangle indicates the range of  $B_x$  for which the  $\varphi_0$ -junction is observed.

phase-diffusive regime, such that no hysteresis is observed (Fig. 2a, right panel). This allows probing of the phase response by applying a finite  $I_{\text{bias}} = 100\text{--}500 \text{ pA}$  close to  $I_{\text{ref}}$  and monitoring the voltage drop  $V$ , across the SQUID as a function of gate voltage  $V_2$  and flux  $\Phi$  (see the lower panels in Fig. 2a,b as well as Supplementary Information Section 2).

In this QD regime, the phase of the SQUID pattern depends crucially on the dot occupation number (Fig. 2b). For example, for  $V_2 \approx -247 \text{ mV}$ , the measured voltage oscillates as a function of  $\Phi$  with a particular phase (purple coloured line in Fig. 2b lower panel). When  $V_2$  is increased to around  $-240 \text{ mV}$ , the oscillations disappear and the overall voltage drops as the charge degeneracy point is reached. By increasing  $V_2$  further, the oscillations recover with an extra  $\pi$  phase corresponding to the sign reversal of the supercurrent in a QD<sup>21</sup> (light blue line in Fig. 2b lower panel). The change of phase by  $\pi$  is repeated for several consecutive charge states.

The change in phase measured for zero in-plane field occurs owing to the change in the electron parity of the ground state. In a simple physical picture, for odd QD occupancy, the order of electrons forming a Cooper pair is reversed in the process of co-tunnelling through a single quantum dot orbital. This results in the sign reversal of the supercurrent and the observed  $\pi$  shift, as previously reported in ref. 21. Note, however, that even if the phase of the ground state is changed,  $I(\varphi = 0)$  remains zero, which is anticipated as time-reversal symmetry is preserved.

Finite magnetic fields can substantially modify this simple picture in two ways. First, the QD levels split by Zeeman energy, which results in different co-tunnelling rates for spin-up and spin-down electrons, and therefore breaks time-reversal symmetry. Second, the spin split levels belonging to different orbitals move closer in energy, which enables more than one orbital to contribute to the co-tunnelling process. This, in turn, combined with strong SOI-induced orbital mixing and asymmetry in the barriers, results in the breaking of chiral symmetry (see Supplementary Section 1)<sup>16</sup>. Under these conditions one can expect an anomalous current and shifts in the phase by an arbitrary  $\varphi_0$  (see Supplementary Section 3 for details on the relation between the anomalous current and  $\varphi_0$ ).

For finite in-plane magnetic fields we find regimes in which the shifts of the SQUID pattern are different from 0 or  $\pi$ . Instead, the shifts take non-universal values depending on the specific QD configuration and magnetic field direction and strength (Fig. 3). Figure 3a,b shows an example taken close to the QD charge degeneracy point. The shift in SQUID response between the two Coulomb blockade regions is approximately  $0.7\pi$ . This value is considerably different from the value  $\pi$  observed for the same QD regime when the in-plane field is zero (compare the data in Fig. 3b,d with the data in Fig. 2b). Note also that, although effects related to finite temperature have an impact on the critical current values, and in general on the values and visibility of the SQUID response, they do not contribute to any phase offset (see Supplementary Section 4).

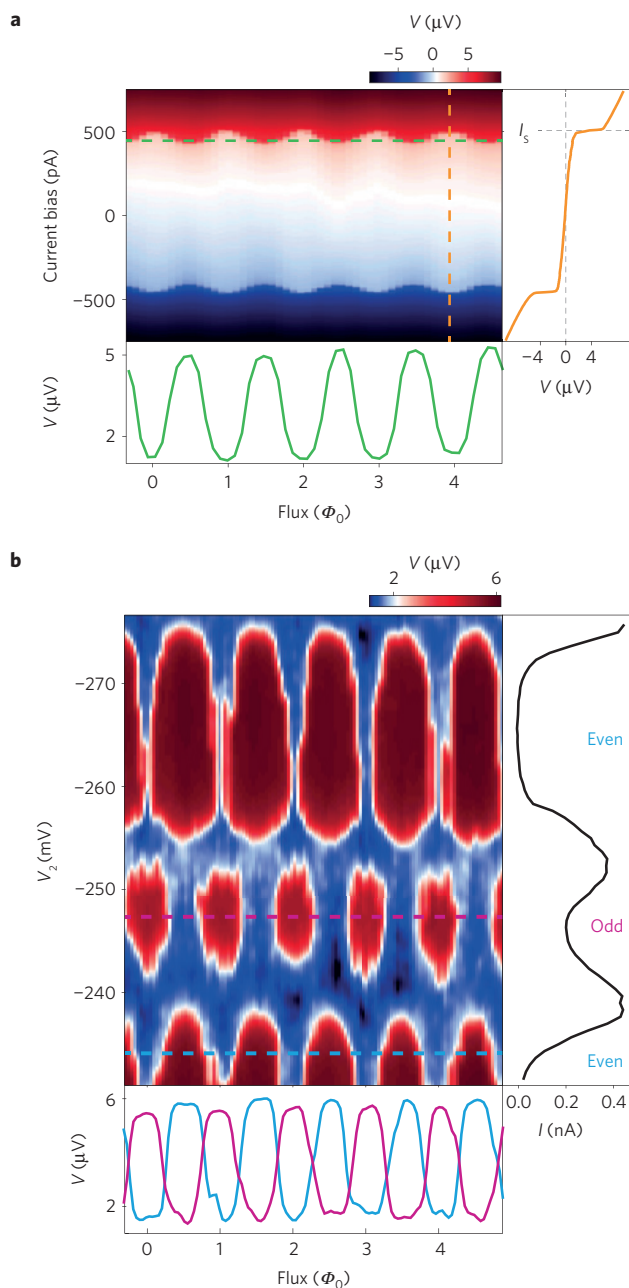


**Figure 2 | Nanowire SQUID characterization for  $B_{\text{in-plane}} = 0$ .** **a**, Voltage across the SQUID,  $V$ , as a function of bias current  $I_{\text{bias}}$  and flux  $\Phi$  through the SQUID. The right panel shows  $V$  versus  $I_{\text{bias}}$  measured at  $\Phi = 4\Phi_0$  (cut along the orange dashed line). The switching current  $I_s$  separating low- and high-resistance regions is indicated. The lower panel shows voltage versus  $\Phi$  for  $I_{\text{bias}} = 450$  pA (cut across the green dashed line). **b**,  $V$  as a function of  $V_2$  and  $\Phi$  for  $I_{\text{bias}} = 190$  pA. The phase of the SQUID oscillations alternates between 0 and  $\pi$  depending on the electron parity of the ground state of the QD. The right panel shows Coulomb peaks in the voltage bias regime. The bottom panel shows  $V$  versus flux cuts at  $I_{\text{bias}} = 195$  pA for  $V_2 = -247$  mV (purple) and  $V_2 = -233$  mV (light blue).

The measured gate-tunable phase shift directly implies a finite  $\varphi_0$ , different from 0 or  $\pi$ , for at least one of the Coulomb blockade regions. Importantly, this shift cannot be explained by simple higher-harmonic terms in the JJ current–phase relation which can occur in various semiconductor-based junctions<sup>22–25</sup>. Even if such terms were present, as long as  $I(-\varphi) = -I(\varphi)$ , the SQUID response would have to be symmetric around the points corresponding to

integer values of the threaded flux. As this is clearly not the case in the data shown in Fig. 3, the  $I(-\varphi) = -I(\varphi)$  condition is violated. Note that both junctions in the SQUID are nanowire based and, therefore, phase shifts can occur in the reference junction as well. For this reason, shifts in the SQUID pattern should be interpreted as relative offsets in  $\varphi_0$  of the QD-based junction.

Typically, the phase of the SQUID oscillation is constant within the Coulomb blockade region and changes only at the charge degeneracy points. Depending on the exact gate settings, the phase change appears either as a discrete jump or a continuous transition. In the investigated regimes, we measured jumps when the QD is strongly confined (as in Fig. 3a,b). For a more open QD we observe a continuous change in the phase of the SQUID response as we tune the gate  $G_2$  across the charge degeneracy point (Fig. 3c,d). This behaviour is not fully understood, but we note that transport for a strongly confined QD is dominated by the resonant tunnelling process at the Coulomb peak, and therefore can be very different compared to the transport deep in the blocked regime. This effect is not pronounced for an open QD in which higher-order tunnelling processes are relevant. In the regimes where the SQUID oscillations can be detected along the whole charge transition, we observe a continuously changing phase. Importantly, in all regimes, fields of  $B_{\text{in-plane}} \approx 50$ –150 mT are required to see a noticeable shift in the SQUID response (see Supplementary Section 5). These fields are still around two to four times smaller compared to the critical fields of  $B_{\text{in-plane}} = 200$ –300 mT at which the SQUID response vanishes.

Finally, we examine the magnetic anisotropy dependence of the SQUID pattern, to further study the microscopic origin of the  $\varphi_0$ -junction. The data showing phase shifts between neighbouring charge states for various in-plane magnetic field angles are presented in Fig. 4. Consistently, for many different QD regimes, we observe that the maximum shift of the SQUID pattern is most pronounced when an in-plane field is applied orthogonal to the nanowire. Previous quantum dot experiments have identified this field orientation with the preferential spin–orbit direction  $\mathbf{B}_{\text{SO}}$  for quantum dots<sup>20</sup>. These measurements are consistent with SOI-enabled orbital mixing, which predicts a maximal phase  $\varphi_0$  for  $\mathbf{B}_{\text{in-plane}} \parallel \mathbf{B}_{\text{SO}}$  (refs 5,15,16). Note that other known mechanisms which could in principle lead to additional phase shifts, such as flux penetrating the JJ area, are not consistent with the observed data (see Supplementary Sections 6 and 7 for a more detailed discussion).

In summary, we demonstrated a gate-tunable Josephson  $\varphi_0$ -junction. Results presented here imply that the breaking of the underlying symmetries can be achieved in superconductor–quantum dot structures while maintaining coherent transport of Cooper pairs. In this context, our experiment is directly related to the efforts of studying triplet superconductivity and superconducting spintronics<sup>26</sup> as well as in achieving topological superconducting phase in quantum dots coupled to an *s*-wave superconductor<sup>16,27–32</sup>. Aside from that, a gate-tunable phase offset may open novel possibilities for the realization of electrically controlled flux- and phase-based quantum bits<sup>33</sup>, superconducting computer memory components<sup>34</sup>, as well as superconducting ‘phase’ batteries and rectifiers<sup>4,35</sup>. Finally, we note that other one-dimensional materials, such as carbon nanotubes, where spin–orbit interaction is strong owing to the curvature of the tube, may be explored in the context of  $\varphi_0$ -junctions<sup>36</sup>.

## Methods

Methods, including statements of data availability and any associated accession codes and references, are available in the [online version of this paper](#).

Received 30 November 2015; accepted 23 March 2016; published online 2 May 2016; corrected after print 2 September 2016

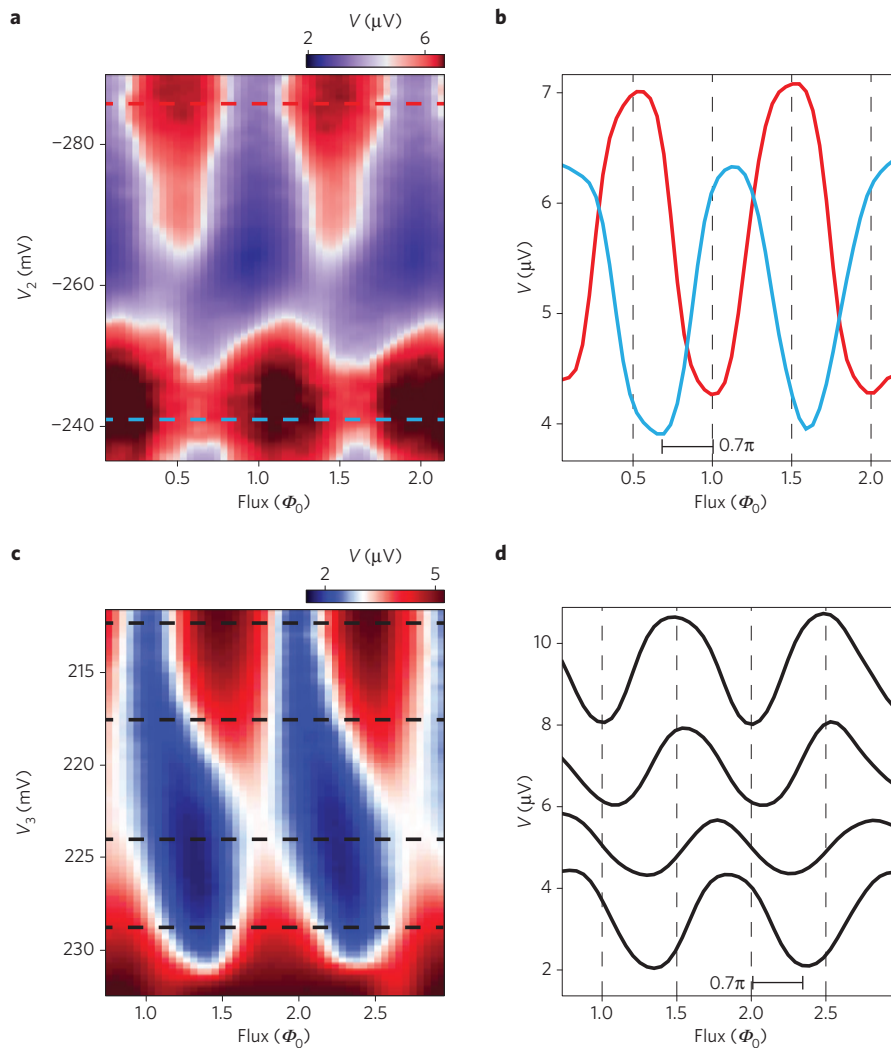


**Figure 3 | Observation of a continuous phase change in the Josephson  $\phi_0$ -junction for finite  $B_{\text{in-plane}}$ .** **a,c**,  $V$  as a function of  $V_2$  (**a**) and  $V_3$  (**c**) and the flux at fixed current bias ( $I_{\text{bias}} = 470$  pA,  $B_{\text{in-plane}} = 120$  mT and  $\theta = -135^\circ$  for **a**;  $I_{\text{bias}} = 240$  pA,  $B_{\text{in-plane}} = 75$  mT and  $\theta = -35^\circ$  for **c**). Here,  $\theta$  is the angle between the direction of the in-plane magnetic field and the nanowire axis. In contrast to the data taken at zero in-plane magnetic field, the phase shift of the voltage oscillations in flux is tunable with gate voltage ( $V_2$  in **a**;  $V_3$  in **c**). **b,d**,  $V$  versus flux for values of  $V_2$  (**b**) or  $V_3$  (**d**), marked by the respective dashed lines on **a** and **c**, showing phase shifts. In **b**, the red curve is taken at  $V_2 = -285$  mV and  $I_{\text{bias}} = 460$  pA and the blue curve at  $V_2 = -240$  mV and  $I_{\text{bias}} = 470$  pA. The relative offset from the two curves is  $0.35 \pm 0.1\Phi_0$ . In **d**, the curves (from top to bottom) are cuts from **c** taken at  $V_3$  values of 213 mV, 218 mV, 225 mV and 229 mV. The corresponding offsets in phase compared to the top curve are  $(0.1 \pm 0.05)\Phi_0$ ,  $(0.3 \pm 0.05)\Phi_0$  and  $(0.4 \pm 0.05)\Phi_0$ . Note that in the QD regime shown in **c** and **d** we used gate  $G_3$  for tuning.

**References**

- Josephson, B. D. Possible new effects in superconductive tunnelling. *Phys. Lett.* **1**, 251–253 (1962).
- Yip, S.-K., De Alcantara Bonfim, O. F. & Kumar, P. Supercurrent tunneling between conventional and unconventional superconductors: a Ginzburg–Landau approach. *Phys. Rev. B* **41**, 11214–11228 (1990).
- Buzdin, A. Direct coupling between magnetism and superconducting current in the Josephson  $\phi_0$ -junction. *Phys. Rev. Lett.* **101**, 107005 (2008).
- Reynoso, A. A., Usaj, G., Balseiro, C. A., Feinberg, D. & Avignone, M. Anomalous Josephson current in junctions with spin polarizing quantum point contacts. *Phys. Rev. Lett.* **101**, 107001 (2008).
- Zazunov, A., Egger, R., Jonckheere, T. & Martin, T. Anomalous Josephson current through a spin–orbit coupled quantum dot. *Phys. Rev. Lett.* **103**, 147004 (2009).
- Golubov, A. A., Kupriyanov, M. Y. & Il'ichev, E. The current-phase relation in Josephson junctions. *Rev. Mod. Phys.* **76**, 411–469 (2004).
- Krive, I. V., Gorelik, L. Y., Shekhter, R. I. & Jonson, M. Chiral symmetry breaking and the Josephson current in a ballistic superconductor–quantum wire–superconductor junction. *Low Temp. Phys.* **30**, 398–404 (2004).
- Liu, J.-F. & Chan, K. S. Anomalous Josephson current through a ferromagnetic trilayer junction. *Phys. Rev. B* **82**, 184533 (2010).
- Tanaka, Y., Yokoyama, T. & Nagaosa, N. Manipulation of the Majorana fermion, Andreev reflection, and Josephson current on topological insulators. *Phys. Rev. Lett.* **103**, 107002 (2009).
- Dolcini, F., Houzet, M. & Meyer, J. S. Topological Josephson  $\phi_0$  junctions. *Phys. Rev. B* **92**, 035428 (2015).
- Alidoust, M. & Linder, J.  $\varphi$ -state and inverted Fraunhofer pattern in nonaligned Josephson junctions. *Phys. Rev. B* **87**, 060503 (2013).
- Bergeret, F. S. & Tokatly, I. V. Theory of diffusive  $\phi_0$  Josephson junctions in the presence of spin–orbit coupling. *Europhys. Lett.* **110**, 57005 (2015).
- Yokoyama, T., Eto, M. & Nazarov, Y. V. Anomalous Josephson effect induced by spin–orbit interaction and Zeeman effect in semiconductor nanowires. *Phys. Rev. B* **89**, 195407 (2014).
- Campagnano, G., Lucignano, P., Giuliano, D. & Tagliacozzo, A. Spin–orbit coupling and anomalous Josephson effect in nanowires. *J. Phys. Condens. Matter* **27**, 205301 (2015).
- Dell'Anna, L., Zazunov, A., Egger, R. & Martin, T. Josephson current through a quantum dot with spin–orbit coupling. *Phys. Rev. B* **75**, 085305 (2007).
- Brunetti, A., Zazunov, A., Kundu, A. & Egger, R. Anomalous Josephson current, incipient time-reversal symmetry breaking, and Majorana bound states in interacting multilevel dots. *Phys. Rev. B* **88**, 144515 (2013).

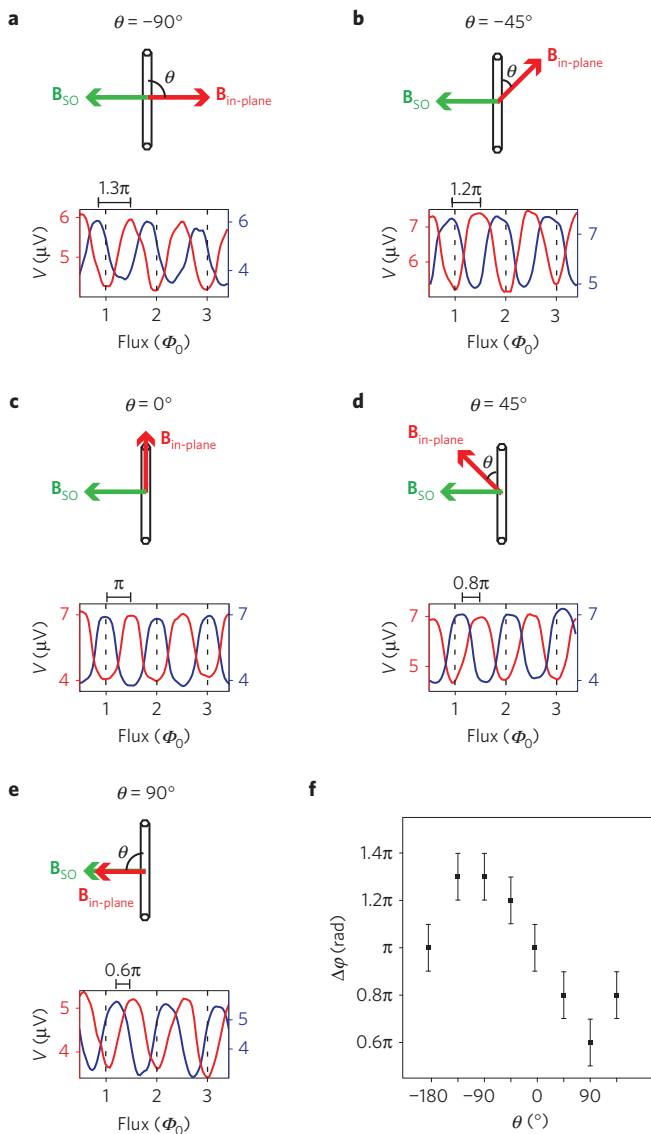


**Figure 4 | Anisotropy of the SQUID phase shift for various angles of  $B_{\text{in-plane}}$ .** **a–e**, Voltage versus flux for different orientations of  $B_{\text{in-plane}} = 120$  mT. Red and blue curves in each panel are taken at two neighbouring charge occupations, as in Fig. 3a, and the corresponding relative phase shift between is marked above each panel. The maximum shift from  $\pi$  was obtained when the field is perpendicular to the wire, as expected from the SOI-enabled orbital mixing (see also Supplementary Section 5). **f**, Phase offset as a function of angle  $\theta$  between the nanowire and  $B_{\text{in-plane}}$ .

17. Goldobin, E., Koelle, D., Kleiner, R. & Mints, R. G. Josephson junction with a magnetic-field tunable ground state. *Phys. Rev. Lett.* **107**, 227001 (2011).
18. Sickinger, H. *et al.* Experimental evidence of a  $\varphi$  Josephson junction. *Phys. Rev. Lett.* **109**, 107002 (2012).
19. Fasth, C., Fuhrer, A., Samuelson, L., Golovach, V. N. & Loss, D. Direct measurement of the spin–orbit interaction in a two-electron InAs nanowire quantum dot. *Phys. Rev. Lett.* **98**, 266801 (2007).

20. Nadj-Perge, S., Frolov, S. M., Bakkers, E. P. A. M. & Kouwenhoven, L. P. Spin-orbit qubit in a semiconductor nanowire. *Nature* **468**, 1084–1087 (2010).
21. van Dam, J. A., Nazarov, Y. V., Bakkers, E. P. A. M., De Franceschi, S. & Kouwenhoven, L. P. Supercurrent reversal in quantum dots. *Nature* **442**, 667–670 (2006).
22. Della Rocca, M. L. *et al.* Measurement of the current-phase relation of superconducting atomic contacts. *Phys. Rev. Lett.* **99**, 127005 (2007).
23. Pillet, J.-D. *et al.* Andreev bound states in supercurrent-carrying carbon nanotubes revealed. *Nature Phys.* **6**, 965–969 (2010).
24. Chang, W., Manucharyan, V. E., Jespersen, T. S., Nygård, J. & Marcus, C. M. Tunneling spectroscopy of quasiparticle bound states in a spinful Josephson junction. *Phys. Rev. Lett.* **110**, 217005 (2013).
25. Cleuziou, J.-P., Wernsdorfer, W., Bouchiat, V., Ondarçuhu, T. & Monthieux, M. Carbon nanotube superconducting quantum interference device. *Nature Nanotech.* **1**, 53–59 (2006).
26. Linder, J. & Robinson, J. W. A. Superconducting spintronics. *Nature Phys.* **11**, 307–315 (2015).
27. Leijnse, M. & Flensberg, K. Parity qubits and poor man’s Majorana bound states in double quantum dots. *Phys. Rev. B* **86**, 134528 (2012).
28. Fulga, I. C., Haim, A., Akhmerov, A. R. & Oreg, Y. Adaptive tuning of Majorana fermions in a quantum dot chain. *New J. Phys.* **15**, 045020 (2013).
29. Konschelle, F., Tokatly, I. V. & Bergeret, F. S. Theory of the spin-galvanic effect and the anomalous phase shift  $\varphi_0$  in superconductors and Josephson junctions with intrinsic spin–orbit coupling. *Phys. Rev. B* **92**, 125443 (2015).
30. Zyuzin, A., Alidoust, M. & Loss, D. Josephson junction through a 3D topological insulator with helical magnetization. Preprint at <http://arXiv.org/abs/1511.01486> (2015).
31. San-Jose, P., Prada, E. & Aguado, R. Mapping the topological phase diagram of multiband semiconductors with supercurrents. *Phys. Rev. Lett.* **112**, 137001 (2014).
32. Marra, P., Citro, R. & Braggio, A. Signatures of topological phase transitions in Josephson current-phase discontinuities. Preprint at <http://arXiv.org/abs/1508.01799> (2015).
33. Padurariu, C. & Nazarov, Y. V. Theoretical proposal for superconducting spin qubits. *Phys. Rev. B* **81**, 144519 (2010).
34. Gingrich, E. C. *et al.* Controllable  $0-\pi$  Josephson junctions containing a ferromagnetic spin valve. *Nature Phys.* **12**, 564–567 (2016).
35. Reynoso, A. A., Usaj, G., Balseiro, C. A., Feinberg, D. & Avignon, M. Spin-orbit-induced chirality of Andreev states in Josephson junctions. *Phys. Rev. B* **86**, 214519 (2012).
36. Delagrangue, R. *et al.*  $0-\pi$  quantum transition in a carbon nanotube Josephson junction: universal phase dependence and orbital degeneracy. Preprint at <http://arxiv.org/abs/1601.03878> (2016).

## Acknowledgements

We gratefully acknowledge R. N. Schouten, S. M. Frolov, D. I. Pikulin, A. Geresdi, K. Zuo, V. Mourik, A. R. Akhmerov, M. Wimmer, Y. V. Nazarov and C. W. J. Beenakker for useful discussions and their help. This work has been supported by funding from the Netherlands Foundation for Fundamental Research on Matter (NWO/FOM), Microsoft Corporation Station Q and the ERC synergy grant.

## Author contributions

D.B.S. fabricated the sample. D.B.S. and S.N.-P. performed the measurements. D.C., S.R.P. and E.P.A.M.B. grew the InSb nanowires. All authors discussed the data and contributed to the manuscript.

## Additional information

Supplementary information is available in the [online version of the paper](#). Reprints and permissions information is available online at [www.nature.com/reprints](http://www.nature.com/reprints). Correspondence and requests for materials should be addressed to L.P.K.

## Competing financial interests

The authors declare no competing financial interests.

## Methods

**Device fabrication.** The indium antimonide (InSb) wires used in the experiments were grown using the metalorganic vapour phase epitaxy (MOVPE) process<sup>37</sup>. The wires were transferred to a SiO<sub>2</sub> chip with local electrostatic gates made of Ti/Au of thickness 5 nm/10 nm, predefined by means of electron beam lithography. The superconducting contacts were subsequently designed and patterned over the wires, and before deposition the wires were etched in Ar<sup>+</sup> plasma for 120 s to remove native surface oxides. NbTiN was sputtered in conditions similar to those described in ref. 38.

**Measurements.** All measurements are performed in a He3/He4 dilution refrigerator equipped with suitable high-frequency electronic filtering at a base temperature of  $T = 20$  mK. The magnetic fields, both in-plane and for flux bias, are applied by means of a 3-axis vector magnet.

To avoid hysteresis in the magnetic field while performing flux-biased measurements, we first step the magnetic field in the  $y$ -direction to adjust the flux to the desired value. We then set the gate and measure the voltage over our device

for gate values corresponding to different charge states of the quantum dot. Then we step the flux forward and repeat the voltage measurements for the same gate values and so on. Hence, the flux increases monotonically for a data set related to a particular in-plane field value, and we do not suffer from hysteresis from the vector magnet. Our measurements were reproducible, and finite offsets in the SQUID response corresponding to the  $\phi_0$ -junction were observed in three separate cooldowns of the device.

**Data availability.** The authors declare that the data supporting the findings of this study are available within the article and its supplementary information files.

## References

37. Plissard, S. R. *et al.* From InSb nanowires to nanocubes: looking for the sweet spot. *Nano Lett.* **12**, 1794–1798 (2012).
38. Mourik, V. *et al.* Signatures of Majorana fermions in hybrid superconductor–semiconductor nanowire devices. *Science* **336**, 1003–1007 (2012).

## Erratum: Josephson $\varphi_0$ -junction in nanowire quantum dots

D. B. Szombati, S. Nadj-Perge, D. Car, S. R. Plissard, E. P. A. M. Bakkers and L. P. Kouwenhoven

*Nature Physics* **12**, 568–572 (2016); published online 2 May 2016; corrected after print 2 September 2016

In the version of this Letter originally published ref. 34 was not updated and should have read: Gingrich, E. C. *et al.* Controllable  $0-\pi$  Josephson junctions containing a ferromagnetic spin valve. *Nature Phys.* **12**, 564–567 (2016). This has now been corrected in the online versions of the Letter.